Dalton Transactions

Accepted Manuscript

Dalton Transactions

An international journal of inorganic chemistry

www.rsc.org/dalton

Volume 39 | Number 3 | 21 January 2010 | Pages 657–964

SYNERGY

$E_{electrostatic}$

$E_{induction}$

$E_{dispersion}$

ISSN 1477-9226

RSC Publishing

PAPER
Manzano et al.
Experimental and computational study
of the interplay between C–H/π and
anion–π interactions

COMMUNICATION
Bu et al.
Zinc(ii)-boron(iii)-imidazolate
framework (ZBIF) with unusual
pentagonal channels prepared from
deep eutectic solvent

1477-9226(2010)39:1;1-K

Emissive Cyanide-Bridged Bimetallic Compounds as Building Blocks for Polymeric Antennae

Alejandro Cadranel,[†] Bruno M. Aramburu Trošelj,[†] Shiori Yamazaki,[††]

Pablo Alborés,[†] Valeria D. Kleiman[††] and Luis M. Baraldo.[†]*

[†]Departamento de Química Analítica, Inorgánica y Química Física, INQUIMAE, Facultad de Ciencias Exactas y Naturales, Universidad de Buenos Aires, Pabellón 2, Ciudad Universitaria, C1428EHA, Buenos Aires, Argentina.
[††]Department of Chemistry, University of Florida, Gainesville, FL 32611-7200, USA.

e-mail: baraldo@qi.fcen.uba.ar

ABSTRACT

A series of cyanide-bridged bimetallic compounds of the general formula $[Ru(L)(bpy)(\mu\text{-}NC)(M)]^{2\text{-}/\text{-}/2+}$ (L = tpy, 2,2'-6',2''-terpyridine, or tpm, *tris*(1-pyrazolyl)methane, bpy = 2,2'-bipyridine, M = $Ru^{II}(CN)_5$, $Os^{III}(CN)_5$, $Os^{II}(CN)_5$, $Ru^{II}(py)_4(CN)$, py = pyridine) have been synthesized and fully characterized. Most of them present a MLCT emission (λ = 690-730 nm, Φ = 10^{-3}-10^{-4}) and their photophysical properties resemble the ones of the respective mononuclear Ru(L)(bpy) species. The exception is when M is $Os^{III}(CN)_5$, where an intramolecular electron transfer quenching mechanism is proposed. The conditions that should be meet for avoiding the reductive or oxidative quenching of the excited state are also discussed.

KEYWORDS

Molecular Antenna – Excited States - Cyanide-bridged Complexes – Metal-Metal Interaction – Mixed Valence Complexes –Intervalence Charge Transfer Band – Supramolecular Chemistry – Ruthenium bipyridine

Introduction.

Molecular antennae are fundamental components of any molecular device designed to interact with light, like photovoltaic cells[1,2] and photocatalysts.[3–5] The proper design of these systems requires a detailed understanding of the processes following light absorption, such as the dynamics of the energy transfer between different components of an artificial multichromophoric array.[6] Control over these processes is required in order to prepare systems that could funnel the energy to where it is required to perform a specific function.

Cyanide bridged multimetallic arrays are an attractive option to build molecular antennae. The cyanide bridge promotes efficient mixing between the metal-centered states and opens the way for efficient electron and energy transfer.[7–9] Additionally, unlike other widely used bridges, the cyanide group does not introduce low energy states that may act as electron or energy traps. In a previous report[9] we presented the photophysical properties of four mononuclear compounds [Ru(L)(bpy)(X)] (L = tpy (**a**) or tpm (**b**) and X = CN^- (**1**) and NCS^- (**2**), hereafter **1a-b** and **2a-b**), which are weak MLCT emitters, and the related cyanide bridged bimetallic species [Ru(L)(bpy)(μ-NC)M(CN)$_5$]$^{n-}$ where M = Fe(III) (**3a-b**), Fe(II) (**3a-b^r**), Cr(III) (**4a-b**). In these cases, either low energy iron or chromium-centered *d-d* states or low energy MM'CT states served as pathways for efficient quenching of the Ru(polypy)-centered MLCT emission. Our goal is to develop an inorganic polymer containing several absorbing units (antennae) that may be able to transfer the energy or the charge to the desired fragment of a larger molecular system. Thus, connectors with low energy states that serve as energy traps should be avoided. In this work, we extend our

studies of this family of compounds to new cyanide-bridged bimetallic complexes

$[Ru(L)(bpy)(\mu\text{-}NC)M]^{2\text{-}/\text{-}/2+}$ (M = $Ru^{II}(CN)_5$ (**5a^r-b^r**), $Os^{III}(CN)_5$ (**6a-b**), $Os^{II}(CN)_5$ (**6a^r-b^r**),

$Ru^{II}(py)_4(CN)$ (**7a^r-b^r**), py = pyridine, their structures are shown in Scheme 1 while

chemical formulae and labels are listed in Table 1) which include second and third row

transition metals, and therefore have their metal centered (MC) states at higher energies so

they may not be able to quench the excited state.
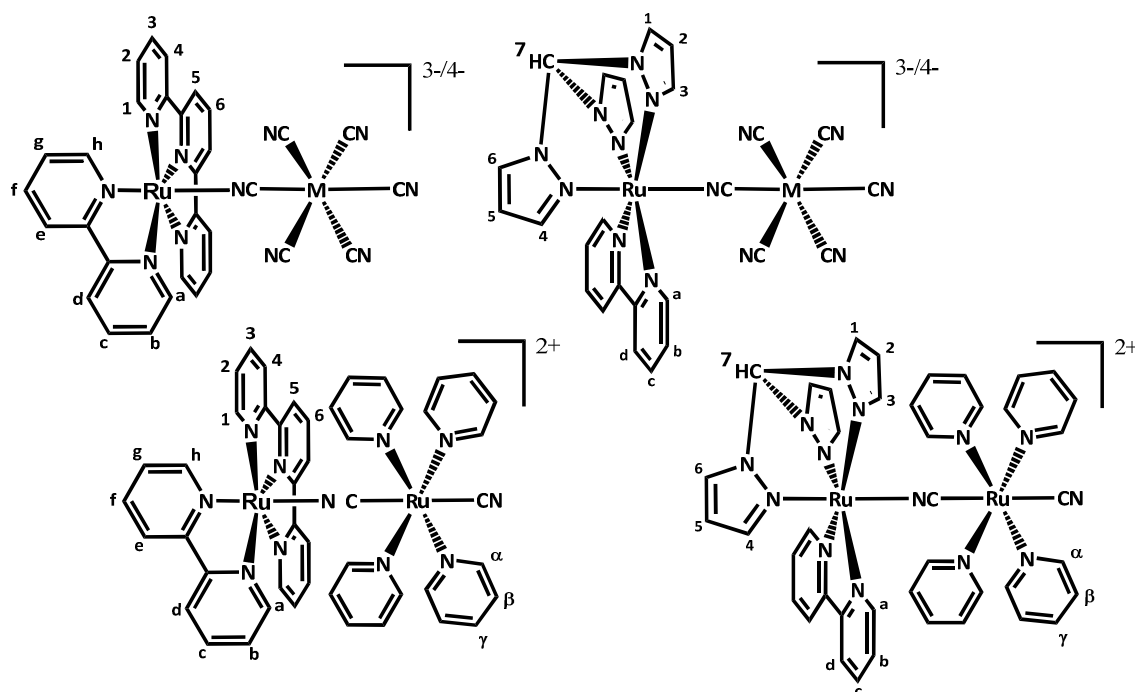
Scheme 1. Sketches of the complexes of the family $[Ru(L)(bpy)(\mu\text{-}NC)M]^{n\text{-}}$ (M = $Ru^{II}(CN)_5$ (**5a^r-b^r**),

$Os^{III}(CN)_5$ (**6a-b**), $Os^{II}(CN)_5$ (**6a^r-b^r**), $Ru^{II}(py)_4(CN)$ (**7a^r-b^r**)). The alphanumeric labels identify the different

H atoms in ^1H NMR.

L	M	Complex
tpy	$Ru^{II}(CN)_5$	**5a**[r]
	$Os^{III}(CN)_5$	**6a**
	$Os^{II}(CN)_5$	**6a**[r]
	$Ru^{II}(py)_4(CN)$	**7a**[r]
tpm	$Ru^{II}(CN)_5$	**5b**[r]
	$Os^{III}(CN)_5$	**6b**
	$Os^{II}(CN)_5$	**6b**[r]
	$Ru^{II}(py)_4(CN)$	**7b**[r]

Table 1. Complexes of the family $[Ru(L)(bpy)(\mu\text{-}NC)M]^{2-/-/2+}$ reported in this work. The numbering scheme

(see ESI Table S1) is consistent with the complexes reported earlier.[9]

Experimental Section.

Materials.

The complexes $K_4[Ru(CN)_6]$,[10] $K_4[Os(CN)_6]$,[11] $(TPP)_3[Os(CN)_6]$,[12] $[Ru^{II}(py)_4(CN)_2]$,[13]

$[Ru(tpm)(bpy)Cl]Cl$,[14] $[Ru(tpm)(bpy)(OH_2)](PF_6)_2$,[14] $[Ru(tpy)(bpy)Cl]Cl$[15] and

$[Ru(tpy)(bpy)(OH_2)](PF_6)_2$,[15] were prepared according to previous reports (TPP$^+$ =

tetraphenylphosphonium). All other reagents were obtained commercially and used without

further purification. Solvents used for UV-visible and electrochemistry measurements were

dried according to literature procedures.[16] The N-tetrabutylammonium hexafluorophosphate

(TBAPF$_6$) used in the cyclic voltammetry experiments was recrystallized from ethanol. All

compounds synthesized were dried in a vacuum desiccator for at least 12 hours prior to

characterization.

Synthesis.

$K_2[Ru(L)(bpy)(\mu\text{-}NC)Ru^{II}(CN)_5]$ (L = tpy **(5a^r)** or tpm **(5b^r)).** These syntheses are a

variation of those described in our previous work[9] for complexes **3a^r-b^r**. A sample with

0.18 mmol of [Ru(L)(bpy)Cl]Cl (L = tpy, 101 mg; L = tpm, 104 mg) and 5 eq. of $K_4[Ru(CN)_6]$ (370 mg) were dissolved in 100 mL of water, and the mixture heated at reflux for 2 hours and 30 minutes. The solvent was evaporated until 20 mL remained and the insoluble products filtered off. 40 mL of methanol were added and a light-red colored solid was found to precipitate. After cooling for 30 minutes in the refrigerator, the solid was collected by filtration, and the resulting red solution containing the desired product was preserved. To recover the product, the light-red solid was dissolved in a minimum amount of water and precipitated with methanol and cooled down. A white solid was formed and separated by filtration from a red colored solution. Both red solutions were mixed and evaporated to 10 mL. 50mL of diethyl ether were added and the resulting red solid was filtered off, washed with diethyl ether and dried in the dissecator. L = tpy: Yield: 93 mg (53%). Anal. Calcd. for **5a^r.8H$_2$O**: C, 38.4; H, 3.6; N, 15.9. Found: C, 38.8; H, 3.2; N, 15.9.
^{1}H NMR (500 MHz, D$_2$O) δ 10.46 (d, J = 5.5 Hz, 1H, Ha) 8.57 (d, J = 8.0 Hz, 1H, Hd), 8.32 (d, J = 8.0 Hz, 2H, H5), 8.26 (m, 4H, Hc+He+H4), 8.11 (ddd, J = 7.0, 5.5, 1.0 Hz, 1H, Hb), 7.85 (t, J = 8.0 Hz, 1H, H6), 7.81 (dd, J = 5.5, 1 Hz, 2H, H1), 7.76 (ddd, J = 8.0, 8.0, 1.0 Hz, 2H, H3), 7.59 (ddd, J = 8.0, 8.0, 1.0 Hz, 1H, Hf), 7.23 (ddd, J = 8.0, 5.5, 1.0 Hz, 2H, H2), 7.00 (d, J = 6.0 Hz, 1H, Hh), 6.83 (ddd, J = 8.0, 6.0, 1.0 Hz, 1H, Hg). IR v_{CN} = 2121, 2082(sh), 2052 cm^{-1}. L = tpm: Yield: 65 mg (39%). Anal. Calcd. for **5b^r.6H$_2$O**: C, 34.1; H, 3.3; N, 21.4. Found: C, 34.1; H, 3.0; N, 21.1. ^{1}H NMR (D$_2$O, 500MHz) δ (ppm): 9.39 (s, 1H, H7), 8.66 (d, J = 6.0 Hz, 2H, Ha), 8.54 (d, J = 8.0 Hz, 2H, Hd), 8.42 (d, J = 3.0 Hz, 2H, H1), 8.41 (d, J = 3.0 Hz, 1H, H4), 8.20 (s, 2H, H3), 8.08 (ddd, J = 8.0, 7.0, 1.0 Hz, 2H, Hc), 7.48 (dd, J = 7.0, 7.0 Hz, 2H, Hb), 6.54 (s, 1H, H6), 6.51 (s, 2H, H2), 6.14 (d, J = 3.0 Hz, 1H, H5). IR v_{CN} = 2122, 2086, 2050 cm^{-1}. In both cases, the amount of hydration molecules was confirmed by TGA (ESI Figures S1 and S2).

(TPP)[(L)(bpy)Ru(μ-NC)Os^{III}(CN)$_5$] (L = tpy (6a) or tpm (6b). The procedure is analogous to that of complexes **3a-b** and **4a-b** reported in reference 9, yielding dark violet crystalline solids. L = tpy: Yield: 65 mg (29 %). Anal. calcd. for **6a.4H$_2$O**: C, 52.9; H, 3.8; N, 12.3. Found: C, 52.9; H, 3.6; N, 12.2. IR ν_{CN} = 2122, 2105, 2086, 2036, 2026 cm^{-1}. L = tpm: Yield: 55 mg (24 %). Anal. calcd. for **6b.8H$_2$O**: C, 46.2; H, 4.2; N, 15.1. Found: C, 46.6; H, 3.9; N, 15.1. IR ν_{CN} = 2122, 2106(sh), 2090, 2070, 2043, 2026 cm^{-1}. In both cases, the presence of water hydration molecules was also detected in the X-ray structures, although in a different amount.

K$_2$[Ru(L)(bpy)(μ-NC)Os^{II}(CN)$_5$] (L = tpy (6a^r) or tpm (6b^r). The procedure is analogous to that of complexes **5a^r-b^r**, replacing potassium hexacyanoruthenate with K$_4$[Os(CN)$_6$], yielding red-orange solids. L = tpy: Yield: 81 mg (42%). Anal. Calcd. for **6a^r.9H$_2$O**: C, 34.6; H, 3.4; N, 14.3. Found: C, 34.7; H, 2.9; N, 14.0.^{1}H NMR (500 MHz, D$_2$O) δ 10.41 (dd, J = 5.5, 0.5 Hz, 1H, Ha), 8.56 (d, J = 8.0 Hz, 1H, Hd), 8.30 (d, J = 8.0 Hz, 2H, H5), 8.25 (m, 4H, Hc + He + H4), 8.11 (ddd, J = 7.5, 5.5, 1.5 Hz, 1H, Hb), 7.83 (t, J = 8.0 Hz, 1H, H6), 7.80 (d, J = 5.5 Hz, 2H, H1), 7.75 (ddd, J = 8.0, 8.0, 1.5 Hz, 2H, H3), 7.59 (ddd, J = 7.5, 7.5, 1.5 Hz, 1H, Hf), 7.24 (ddd, J = 8.0, 5.5, 1.5 Hz, 2H, H2), 7.02 (d, J = 5.5 Hz, 1H, Hh), 6.83 (ddd, J = 7.5, 5.5, 1.5 Hz, 1H, Hg). IR ν_{CN} = 2122, 2077, 2040 cm^{-1}. L = tpm: Yield: 63 mg (31 %). Anal. Calcd. for **6b^r.12H$_2$O**: C, 28.1; H, 3.8; N, 17.6. Found: C, 29.0; H, 4.1; N, 17.7. ^{1}H NMR (500 MHz, D$_2$O) δ 8.60 (d, J = 6.0 Hz, 2H, Ha), 8.51 (d, J = 8.0 Hz, 2H, Hd), 8.40 (d, J = 3.0 Hz, 2H, H1), 8.38 (d, J = 3.0 Hz, 1H, H4), 8.13 (d, J = 1.0 Hz, 2H, H3), 8.04 (ddd, J = 8.0, 7.0, 1.0 Hz, 2H, Hc), 7.43 (dd, J = 7.0, 6.0 Hz, 2H, Hb), 6.46 (dd, J = 2.0, 2.0 Hz, 2H, H2), 6.44 (d, J = 3.0 Hz, 1H, H6), 6.03 (dd, J = 3.0, 3.0 Hz, 1H, H5). IR ν_{CN} = 2121, 2083, 2040 cm^{-1}.

[(L)(bpy)Ru(μ-NC)Ru^{II}(py)$_4$(CN)](PF$_6$)$_2$ (L = tpy (7a^r) or tpm (7b^r)). 0.14 mmol of [Ru(L)(bpy)OH$_2$](ClO$_4$)$_2$ (L = tpy, 100 mg, L = tpm, 96,4 mg) and 5 eq. of [Ru(py)$_4$(CN)$_2$] (332 mg) were suspended in 100 mL of water and heated at reflux for 2 hours. After the mixture cooled down, the solvent was completely removed with a rotary evaporator. The remaining solid was dissolved in a minimum volume of methanol and loaded on a Sephadex LH-20 column (l = 60 cm, ϕ = 4 cm) packed and eluted with methanol. The third of the four fractions obtained presented a dark brown (L = tpy) or deep orange (L = tpm) color and was evaporated until dryness. The solid was dissolved in a minimum volume of methanol and 5 mL of an aqueous saturated solution of NH$_4$PF$_6$ were added. A brown (L = tpy) or orange (L = tpm) solid was collected by filtration, and dried in desiccator. L = tpy: Yield: 72 mg (36 %). Anal. Calcd. for **7a^r.10H$_2$O**: C, 39.5; H, 4.2; N, 10.8. Found: C, 39.4; H, 3.9; N, 11.1. ^{1}H NMR (500 MHz, CD$_3$CN) δ (ppm) 9.64 (ddd, J = 5.5, 1.5, 1.0 Hz, 1H, Ha), 8.62 (d, J = 8.0 Hz, 1H, Hd), 8.48 (d, J = 8.0 Hz, 2H, H5), 8.36 (ddd, J = 8.0, 1.5, 1 Hz, 2H, H4), 8.36 (m, 1H, He), 8.29 (ddd, J = 8.0, 8.0, 1.5 Hz, 1H, Hc), 8.18 (t, J = 8.0 Hz, 1H, H6), 8.05 (dd, J = 6.5, 1.5 Hz, 8H, Hα), 7.95 (ddd, J = 8.0, 8.0, 1.5 Hz, 2H, H3), 7.82 (ddd, J = 8.0, 5.5, 1.5 Hz, 1H, Hb), 7.79 (ddd, J = 8.0, 8.0, 1.5 Hz, 1H, Hf), 7.72 (ddd, J = 5.5, 1.5, 1.0 Hz, 2H, H1), 7.69 (tt, J = 8.0, 1.5 Hz, 4H, Hγ), 7.39 (ddd, J = 6.0, 1.5, 1.0 Hz, 1H, Hh), 7.32 (ddd, J = 8.0, 5.5, 1.5 Hz, 2H, H2), 7.06 (ddd, H = 8.0, 6.0, 1.5 Hz, 1H, Hg), 6.99 (dd, J = 8.0, 6.5 Hz, 8H, Hβ). IR ν$_{CN}$ = 2106(sh), 2070 cm^{-1}. L = tpm: Yield: 55 mg (29 %). The presence of water hydration molecules was also detected in the X-ray structure, although in a different amount. Anal. Calcd. for **7b^r.6H$_2$O**: C, 37.7; H, 3.8; N, 14.6. Found: C, 37.9.0; H, 4.3; N, 14.6. ^{1}H NMR (CD$_3$CN, 500MHz) δ (ppm): 8.90 (s, 1H, H7), 8.62 (ddd, J = 5.0, 2.0, 0.5 Hz, 2H, Ha), 8.40 (dd, J = 3.0, 1.0 Hz, 2H, H1), 8.38 (ddd, J = 8.0,

1.0, 0.5 Hz, 2H, Hd), 8.30 (dd, J = 2.0, 1.0, 2H, H3), 8.10 (dd, J = 6.0, 1.5 Hz, 8H, Hα),

8.08 (dd, J = 8.0, 2.0 Hz, 2H, Hc), 8.07 (d, J = 1.5 Hz, 1H, H4), 7.67 (tt, J = 8.0, 1.5 Hz,

4H, Hγ), 7.51 (ddd, J = 8.0, 5.0, 1.0 Hz, 2H, Hb), 6.98 (dd, J = 8.0, 6.0 Hz, 8H, Hβ), 6.70

(dd, J = 3.0, 0.5 Hz, 1H, H6), 6.67 (dd, J = 3.0, 2.0 Hz, 2H, H2), 6.29 (dd, J = 3.0, 1.5 Hz,

1H, H5). IR v_{CN} = 2107(sh), 2069 cm^{-1}.

Characterization

IR spectra were collected with a Nicolet FTIR 510P instrument, as KBr pellets. UV-visible

spectra were recorded with a Hewlett-Packard 8453 diode array spectrometer in the range

between 190 and 1100. NMR spectra were measured in a Bruker ARX500 spectrometer,

using deuterated solvents from Aldrich. Elemental analyses were performed with a Carlo

Erba 1108 analyzer. Cyclic voltammetry measurements were performed under argon with

milimolar solutions of the compounds, using a TEQ V3 potentiostat and a standard three

electrode arrangement consisting of a glassy carbon disc (area = 9.4 mm^2) as the working

electrode, a platinum wire as the counter electrode and a reference electrode. Depending on

the solvent, the reference electrode was a Ag/AgCl 3M KCl standard electrode (for aqueous

solutions) or a silver wire (for non- aqueous solutions) plus an internal ferrocene (Fc) or

decamethylferrocene (Me$_{10}$Fc) standard for organic solvents. KNO$_3$ 1M and tetra-N-

butylammonium hexaflourophosphate (TBAPF$_6$) 0.1 M were used as supporting

electrolytes in water and non-aqueous media, respectively. All the potentials reported in

this work are referenced to the standard Ag/AgCl saturated KCl electrode (0.197 V vs.

NHE), the conversions being performed by using the accepted values for the Fc$^+$/Fc couple

in different media.[17]

Excitation and emission spectra were recorded in a PTI-Quantamaster spectrofluorometer.

Quantum yields were measured in Argon-saturated solutions using [Ru(bpy)$_3$]$^{2+}$ (Φ = 0,095

in ACN at 25ºC[18]) as reference, correcting by refractive indices when needed. Time-resolved luminescence measurements were made using a PicoQuant FluoTime 100 Compact Fluorescence Lifetime Spectrometer, with a LDH-P-C-375 diode laser centered at 375 nm (300 ps FWHM) as the excitation source and a PMT detector. Since the Φ for emission are very small, the solutions were highly concentrated with O.D. near 1 at the excitation wavelength. Emission spectra measured under these conditions showed no change from those measured for dilute solutions.

X-ray Structure Determination

Crystal structures of compounds **6a-b, 7a^r** were determined with an Oxford Xcalibur, Eos, Gemini CCD area-detector diffractometer using graphite-monochromated Mo-Kα radiation (λ = 0.71069 Å) at 298 K. Data was corrected for absorption with CrysAlisPro, Oxford Diffraction Ltd.,Version 1.171.33.66 analytically by face-indexing in the case of compound **7a^r** and applying an empirical absorption correction using spherical harmonics, implemented in SCALE3 ABSPACK scaling algorithm in the case of compounds **6a-b**. The structures were solved by direct methods with SHELXS-97 and refined by full-matrix least-squares on F^2 with SHELXL-97. Hydrogen atoms were added geometrically and refined as riding atoms with a uniform value of *Uiso*. Hydrogen atoms of solvent water molecules were not located in the Fourier difference map and therefore not included in the modelling. In structures **6a-b** three and two of the water solvent molecules, respectively, were found disordered and refined as two split positions with 0.5:0.5 occupation ratio. In the case of structure **6a** the oxygen atoms of water solvent molecules could not be anisotropically modelled due to refinement instability. Hence, they were kept isotropically refined. Final crystallographic data and values of *R1* and *wR* are listed in Table S2 (ESI) while the main angles and distances are listed in Table 2. CCDC 918817 - 918819 contains

Dalton Transactions Accepted Manuscript

the supplementary crystallographic data for this paper. These data can be obtained free of charge from the Cambridge Crystallographic Data Center via www.ccdc.cam.ac.uk/data_request/cif.

Results.

Synthesis.

As previously observed,[9] the reaction of the precursors $[Ru(L)(bpy)Cl]^+$ with the anions $[M(CN)_6]^{4-/3-}$ proceeds smoothly in methanol and in water. The poor solubility of the hexacyanometallate(II) in methanol simplifies the purification of the bimetallic complexes **5a^r-b^r** and **6a^r-b^r**, which were obtained as water-soluble potassium salts. The higher potentials of ruthenium and osmium complexes allowed us to prepare compounds **5a^r-b^r** and **6a^r-b^r** under air. In the preparation of **7a^r-b^r**, $[Ru(L)(bpy)(OH_2)]^{2+}$ was chosen as the starting material instead, because of its higher lability when the substituting species was the neutral complex $[Ru(py)_4(CN)_2]$.

X-ray quality single crystals of the TPP$^+$ salts of **6a-b** were obtained by slow evaporation of concentrated methanol-water solutions, while crystals of the PF$_6^-$ salt of **7a^r** were obtained by slow evaporation of acetonitrile-water solutions. Unfortunately the same procedure on **7b^r** yielded crystals of low quality. We were not able to grow crystals of the potassium salts of **5a^r-b^r** and **6a^r-b^r**.

Crystal Structure Determinations.

The crystal structures of bimetallic complexes **6a-b** and **7a^r** were determined by X-ray crystallography. Table 2 summarizes selected bond distances and angles while their structures are shown in Figure 1.

The coordination spheres around the ruthenium atoms present the usual characteristics of the previously reported $[Ru(tpy)(bpy)X]^{n}$ [19–24] and $[Ru(tpm)(bpy)X]^{n}$ [25–27] compounds. The

N_L-Ru-N_L angle shows considerable distortion from the octahedron in the case of **6a-7a^r** and slighter deviations in the case of **6b**, caused by the planar rigid structure of tpy (**a**) and the more flexible facially coordinating tpm (**b**). The Ru-N distances are within the range expected for a Ru(II)-N(polypyridine bond).[19–27] The tetrapyridinic fragment of **7a^r** presents the usual propeller-like configuration[13,28,29] with an average tilting angle of 40° (Figure 1).

Complex **7a^r** shows the shorter C-N distance for the bridge in the structurally characterized members of the $[Ru(L)(bpy)(\mu\text{-}NC)M]^n$ family (1.109(13) Å compared to 1.148(6) Å in **6a**), but these bond distances are within the range of reported values for complexes containing the corresponding cyano-fragment.[12-13,29–31] Usually this bond distance is not affected by the nature of the bridged moieties, although elongation of this bond has been observed in the presence of very electron-rich metals.[32]

The presence of the tpm ligand in the complex **6b** leads to an important deviation from linearity of the Ru-NC_{bridge}-M moiety. The Ru-N-C_{bridge} angle is ~163° while the N-C_{bridge}-Os angle is 172°. These angles are more bent compared to those of compound **6a** (169° and 175° respectively), while **7a^r** shows almost a perfect linear arrangement of these atoms. Additionally, while **6a** presents an almost eclipsed configuration of its equatorial ligands, the structures of **6b** and **7a^r** show significant torsion angles of 35° and 16°, respectively, around the cyanide bridge.

Similar diversity of configurations have been observed previously[9] and indicates that the variations observed are not governed by electronic factors, but are the result of different intermolecular interactions in the crystal structures. For example, whereas **6b** shows π-π stacking between the bpy-bpy ligands (d = 3.33 Å) and the tpm-tpm ligands (d =3.34 Å), only the π-π stacking between the tpy-tpy ligands (d = 3.49 Å) is present in **6a** and the

between tpy-py ligands (d = 3.55 Å) in **7a^r** (ESI Figures S3-S6). Similar distances have

been observed for π-π stacking between aromatic rings in compounds containing the

Ru(tpy)(bpy)[20,24] and Ru(tpm)(bpy)[27] moieties.

Complex Salt	6a	6b	7a^r
Distances / Å			
Ru1-N1$_{bridge}$	2.024(4)	2.003 (6)	2.023(9)
N1-C1$_{bridge}$	1.148(6)	1.128 (8)	1.109(13)
Os1-C1$_{bridge}$	2.045(4)	2.087 (9)	-
C1-Ru2 $_{bridge}$	-	-	2.050(12)
Ru1-Os1	5,180	5.123	-
Ru1-Ru2	-	-	5.181
Ru1-N7$_{bpy}$	2.077(4)	2.040(6)	2.048(8)
Ru1-N8$_{bpy}$	2.044(4)	2.031(6)	2.059(9)
Ru1-N9$_{tpy/tpm}$	2.065(4)	2.076(6)	2.068(11)
Ru1-N10$_{tpy/tpm}$	1.961(4)	2.074(6)	1.936(8)
Ru1-N11 $_{tpy/tpm}$	2.074(4)	2.050(6)	2.119(9)
Angles / deg.			
Ru1-N1-C1$_{bridge}$	168.7(4)	163.2(7)	176.1(8)
N1-C1-Os$_{bridge}$	175.3(4)	171.9(7)	-
N1-C1-Ru2$_{bridge}$	-	-	178.3(9)
N7-Ru1-N8$_{bpy}$	78.41(15)	78.5(3)	79.1(3)
N9-Ru1-10$_{tpy/tpm}$	79.42(16)	85.8(2)	78.5(4)
N10-Ru1-N11$_{tpy/tpm}$	79.13(18)	83.3(2)	80.5(4)
N9-Ru1-N11$_{tpm}$	-	86.0(3)	-
N7-Ru1-Os1-C5	1.62	34.98	-
N7-Ru1-Ru2-N5	-	-	16.39

Table 2. Selected bond distances and angles for the compounds **6a-b** and **7a^r**.

Dalton Transactions Accepted Manuscript
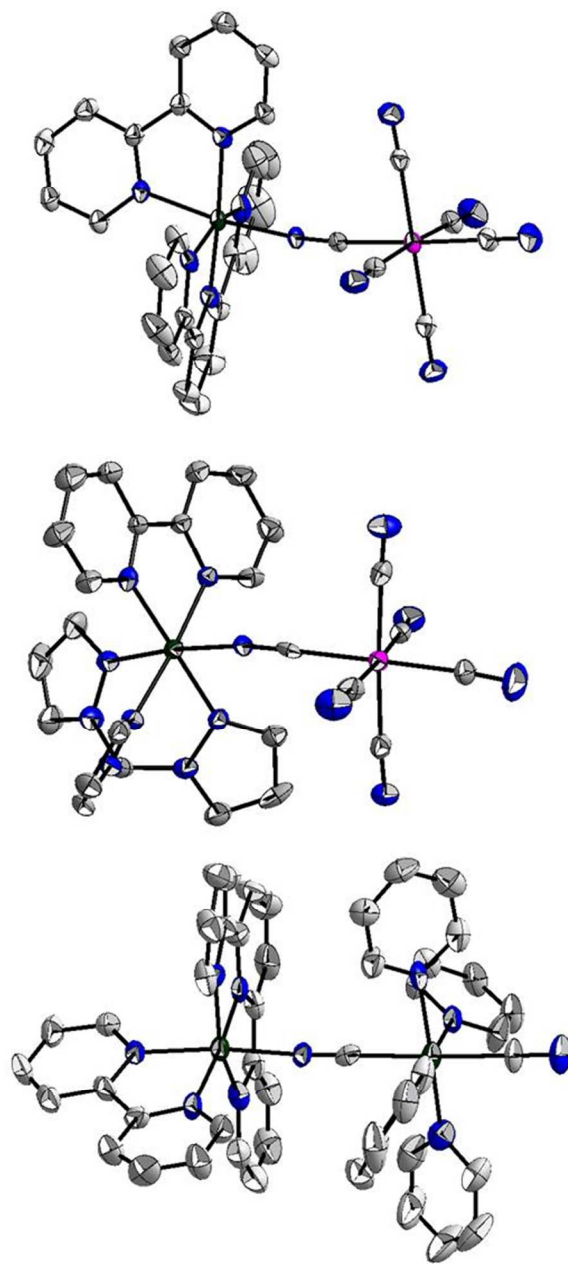
Figure 1. Crystal structures of the complexes **6a** (top), **6b** (center) and **7a^r** (bottom). Ellipsoids represent a 30% displacement probability. Hydrogen atoms, counter ions, and solvent molecules were omitted for clarity.

Electrochemistry

The bimetallic complexes reported here present several active redox center in their structure. Characterization of their redox states not only confirms their structure, but also provides important information to understand the properties of their excited states. Cyclic

voltammograms are shown in Figure 2, while the relevant electrochemical data is presented

in Table 3.
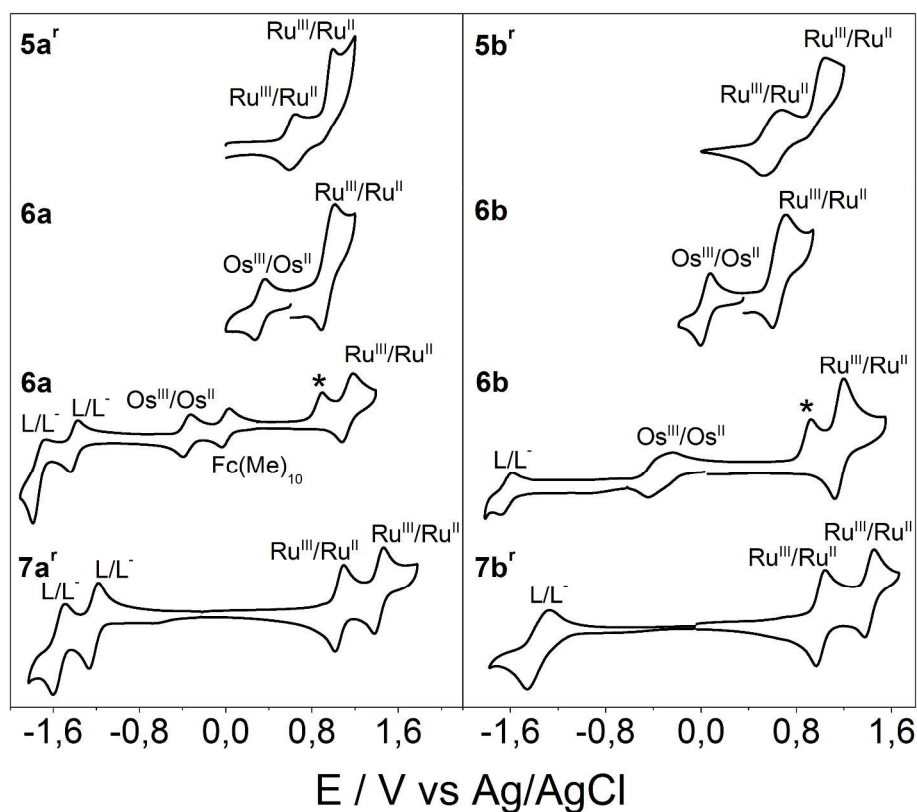
Figure 2. Cyclic voltammograms of complexes, from top to bottom, left panel: **5a**[r] (water), **6a** (water), **6a**

(ACN), **7a**[r] (ACN); right panel: **5b**[r] (water), **6b** (water), **6b** (ACN), **7b**[r] (ACN). The wave labeled with a (∗)

is preliminarily assigned to a Os^{IV}/Os^{III} process.

Complex / Salt	Solvent	$E_{1/2}(Ru)/V$ (ΔE_p/mV)	$E_{1/2}(M)/V$ (ΔE_p/mV)	$E_{1/2}$ (pp)/V (ΔE_p/mV)
5a[r]	H_2O	0.94 (120)	0.61 (150)	nd
5b[r]	H_2O	0.97 (100)	0.60 (55)	nd
6a	H_2O ACN	0.96 (130) 1.13 (100)	0.32 (90) -0.36 (90)	nd -1.41 (70)
6b	H_2O ACN	1.03 (130) 1.16 (70)	0.31 (100) -0.34 (210)	nd -1.63 (100)

7a[r]	ACN	1.42 (90)	1.05 (90)	-1.22 (90)
7b[r]	ACN	1.41 (80)	1.00 (70)	-1.37 (190)
[Ru(tpy)(bpy)(NCS)][+]	ACN	1.04 (90)	-	-1.25 (100)
[Ru(tpm)(bpy)(NCS)][+]	ACN	0.96 (100)	-	-1.42 (110)
[Ru(CN)₆][4-]	H₂O ACN	-	0.97 [a] na	-
[Os(CN)₆][4-]	H₂O ACN	-	0.44 (90) [b] -0.59(90) [b]	-
[Ru(py)₄(CN)₂]	ACN	-	0.77 (90) [c]	-

Table 3. Redox potential for the Ru(III)/Ru(II), M(III)/M(II) and pp/pp⁻ couples for the bimetallic complexes **5-7** and the related monomers in different solvents. a) from reference [10]. b) from reference[12]. c) from reference [13].

Cyclic voltammograms of **5a[r]-b[r]** and **6a[r]-b[r]** were collected in water. These closely related complexes show two reversible or quasi-reversible processes. One of them appears near the potential observed for the Ru(III/II) couple for the corresponding [Ru(L)(bpy)NCS][+] monomer allowing its assignment,[9] while the other, at lower potentials, corresponds to the haxacyanometallate (Table 3). The potential of the latter couple is 300 mV higher in **5a[r]-b[r]** compared to **6a-b** as expected for the replacement of Ru by Os (Table 3).

The electrochemistry of **6a-b** was also explored in acetonitrile (Figure 2). In this solvent the couple for the hexacyanoosmate shifts to lower potentials, as previously observed for [Os(CN)₆][3-12] (Table 3) and other cyanometallate complexes,[33,34] confirming its assignment. Moreover, both show an irreversible anodic wave in acetonitrile, whose potential has a similar solvent dependence (ESI Figure S7) and thus we assign them to another couple associated with the osmium ion (i.e. Os(IV/III) process). To our knowledge, this the first report of such a couple in an osmium hexacyanometallate. We propose that the presence of

15

a coordinated Ru(II) donor stabilizes this redox state, although it is not clear why the process looks irreversible. Further studies are required to establish the nature of this couple. The presence of the additional redox process explains the anodic shift observed for the Ru(III/II) process in **6a-b** in acetonitrile.

Finally, the **7a^r-b^r** complexes show two closely spaced one electron anodic waves (Figure 2), consistent with the two expected Ru(III/II) couples. The assignment of these couples is not straightforward since the potential for the corresponding Ru(III/II) couples in the monomers [Ru(L)(bpy)(NCS)]$^+$ [9] are very similar to that of the Ru(py)$_4$(CN)$_2$ monomer[13] (Table 3). Our preliminary assignment considers that the less anodic process (1.05 and 1.00 V for the dimetallic complexes **7a^r-b^r**, respectively) involves the removal of one electron from the Ru(py)$_4$(CN)$_2$ fragment, whose potential is shifted to higher values due to the coordination of a 2+ fragment to one of the cyanide groups. Similar shifts have been reported in the Ru(py)$_4$(CN)$_2$ potential upon the coordination of a 2+[13] or a 3+[35] fragment. UV-visible and IR spectroelectrochemical studies to confirm these assignments are being carried out in our laboratories.

The bimetallic complexes **6a** and **7a^r** also show two quasi-reversible cathodic waves in acetonitrile related to the reduction of the tpy and the bpy ligands. The former appears at higher potential as expected from the presence of an additional aromatic ring. Complexes **6b** and **7b** instead present only one cathodic wave for the reduction of the bpy ligand.

Photophysics

To gain a deeper understanding of the coupling among the different moieties in the bimetallic complexes, we measured their photophysical properties in acetonitrile and water. Figure 5 shows the absorption spectra of the dimetallic complexes complexes **5b^r**, **6b^r** and **7b^r**. The [Ru(tpm)(bpy)(NCS)]$^+$ monomer has the same coordination environment around

the ruthenium polypyridinic center[9] and thus it is also presented here for comparison. Similar spectra were recorded for the compounds with the tpy ligand as shown in the supplementary information (ESI Figure S8). Absorption maxima and extinction coefficients for all compounds measured (with initial assignments) are listed in Table 4. All these compounds present similar transitions such as the narrow ligand centered (LC) band around 300 nm and the broad MLCT bands in the 440-480 nm region, the latter with π^* acceptor orbitals located on the chelating ligands. An additional MLCT transition is clearly resolved for these complexes around 330 nm, appearing only as a shoulder for the tpy analogues due to the lower energy of the LC signals on those compounds (ESI Figure S8). Bimetallic complexes **7a^r-b^r** (Fig 5 and Figure S8) present an intense absorption feature at ~355 nm corresponding to the Ru(II) $\rightarrow$ π^* (pyridines) MLCT transition. All the charge-transfer processes described up to this point involve dπ orbitals of the ruthenium atom directly attached to the ligand that contains the π^* acceptor orbitals. The presence of two M(II) centers in the bimetallic complexes **5a^r-b^r**, **6a^r-b^r** and **7a^r-b^r** opens the possibility of charge transfer from a metal to a remote ligand (i.e. attached to the second metal) as it has been shown for other bimetallic complexes.[8] The spectra reported here for the Ru(II)M(II) bimetallic complexes follow very closely the pattern observed for the NCS$^-$ monomers **2a-b**.[9] We conclude that the remote MLCT (RMLCT) band must have much lower intensity and do not have a large impact in the absorption profiles. **(**Fig 5 and Figure S8).
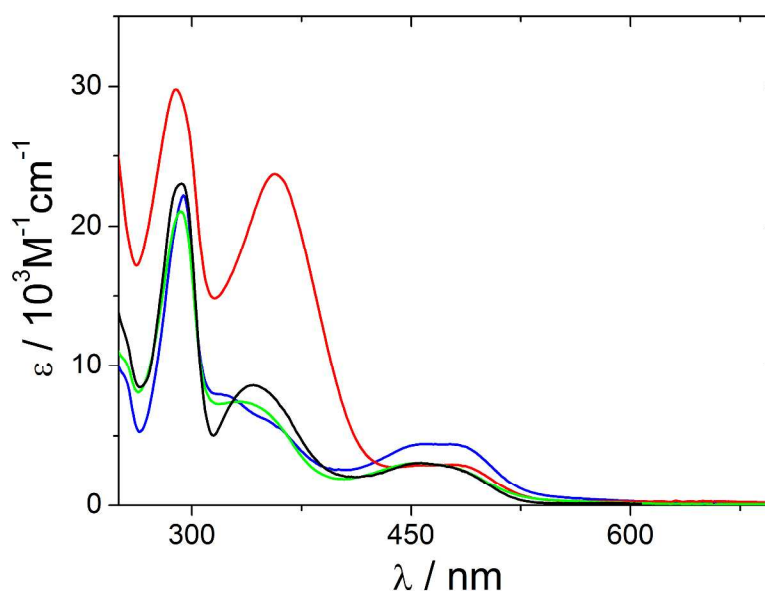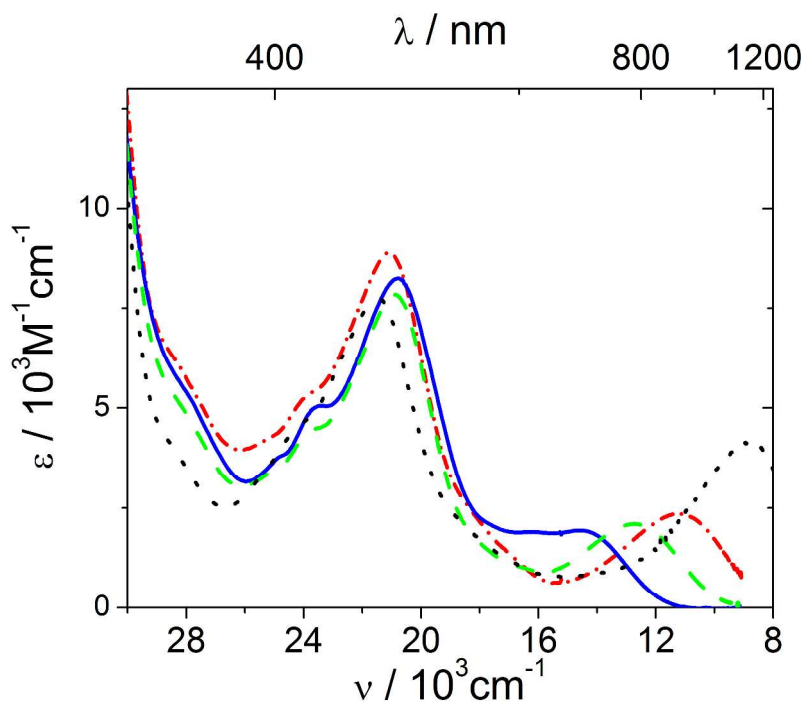
Figure 5. UV-vis absorption of the complexes **5b^r** (green), and **6b^r** (black) in water and **7b^r** in acetonitrile (red). For comparison purposes the spectrum of [Ru(tpm)(bpy)(NCS)]$^+$ in acetonitrile (blue) is also included.

Complex Salt	Solvent	L = tpy (a)				L = tpm (b)			
		$\pi \to \pi^*$		MLCT		$\pi \to \pi^*$		MLCT	
		λ nm	ε M^{-1}cm^{-1}	λ nm	ε M^{-1}cm^{-1}	λ nm	ε M^{-1}cm^{-1}	λ nm	ε M^{-1}cm^{-1}
2	ACN	272	33400	357	6820(sh)	293	22400	322	7910(sh)
		279	34300						
		291	37900	487	9080			458	4410(sh)
		313	30400						
5^r	H$_2$O	273	34600	358	7870(sh)	292	21000	332	7390 (sh)
		281	36300						
		291	40800	486	10420			454	3070
		313	38200						
6	ACN	275	32800	---	----	290	31400	331	5470
		----	------						
		291	32400	481	8280			443	3115
		313	30800						
6^r	H$_2$O	273	39200	358	8750(sh)	293	23000	342	8600
		281	41200						
		291	45500	485	10830			456	3080
		313	40800						
7^r	ACN	274	31300	353	21220	289	29800	357	23680
		282	34100						
		291	35600	479	7440			478	2960
		314	37200						

Table 4. UV-vis absorption data for the complexes reported. For comparison purposes the data for **2** [Ru(L)(bpy)(NCS)]$^+$ is also included.[9]

Compounds **6a-b** exhibit an additional very broad and weak band at lower energies, which is absent for **6a^r-b^r** and whose position depends strongly on the solvent (Table 5, Figures 6 and S9). In acetonitrile, their maxima are located at 685 nm and 718 nm, for **6a-b** respectively. The energy of this transition correlates well with the difference between the redox potential of ruthenium and osmium (ESI Figure S10), and therefore we assign it to a Ru(II) → Os(III) MM'CT transition. When compared to their Ru-Fe analogues (for example, compounds **3a-b** in reference 9), the electronic mixing between the metallic centers is expected to be greater for the Ru-Os complexes due to the larger extension of their dπ orbitals. The values of the coupling term H$_{12}$, arisen from the Mulliken-Hush expression[36–38] and shown in Table 5, are in agreement with this expectation as they are among the larger ones reported for a cyanide bridged system.[8,35,39–42] These results indicate a substantial mixing between the dπ orbitals of the metallic ions ($\alpha^2 = 3.68\times10^{-2}$ for **6a** and $\alpha^2 = 7.17\times10^{-2}$ for **6b** in water). The mixed valence species **5a-b** and **7a-b** will be further studied by spectroelectrochemistry and reported in a forthcoming article.

Figure 6. Vis-NIR absorption of the complexes **6a** in water (black dotted line), methanol (red dash-dotted line), ethanol (green dashed line) and acetonitrile (blue solid line).

Solvent	MM'CT ν/10³cm⁻¹ (ε/10³ M⁻¹cm⁻¹)		$H_{12}{}^a$ / cm⁻¹			
	6a	**6b**	**6a**	**6b**	**3b[b]**	**3b[b]**
ACN	14.6 (2000) (sh)	13.9 (1800)	nd	1083	nd	nd
EtOH	12.7 (2100)	11.9 (2200)	1306	1154	nd	757
MeOH	11.2 (2300)	10.3 (2600)	1302	1282	973	814
H₂O	8.8 (4100)	8.5 (7400)	1689	2263	1303	1213

Table 5. MM'CT transition energies for the mixed-valence species **6a** and **6b**. a) $H_{ab} = \alpha\nu_{max}$, $\alpha^2 = \frac{4.0 \times 10^{-4} \int \varepsilon(\nu)d\nu}{\nu_{max}r_{12}^2}$ and r_{12} is the crystallographic distance between the metallic ions. b) Data for compounds **3a** ([Ru(tpy)(bpy)μ-NC)Fe^{III}(CN)$_5$]⁻) and **3b** ([Ru(tpm)(bpy)(μ-NC)Fe^{III}(CN)$_5$]⁻) were taken from reference 9.

Remarkably, most of the bimetallic molecules reported here show emission at room temperature, with no evidence of photodegradation. Their wavelength of maximum emission, quantum yields and lifetimes are listed in Table 6, while their emission and

excitation spectra are presented in Figure 7. Lifetimes (between 10 and 50 ns) and emission quantum yields (ca. 1×10^{-3}) are similar to those reported for the closely related monomers[19–24,43,44] and points to the triplet MLCT of the ruthenium polypiridine as the emissive state. The preservation of these photophysical properties indicates that addition of a second metal-ion from the 2nd or 3rd transition series (with a d^6 configuration) does not introduce competitive non-radiative pathways. In all the reported systems the excitation spectra matches very well the absorption spectra, which reveals an efficient population of the MLCT state, mainly triplet in character, upon light absorption.

Within each series (L = tpy or L = tpm), the wavelength of maximum emission correlates roughly with the charge of the group occupying the sixth position. When the group is neutral (**7a^r-b^r**), emission occurs at the high-energy end of the spectrum becoming red shifted when the ligand has a single negative charge (**2a-b**)[9] and emitting at even lower energies when the group has multiple negative charges (**5a^r-b^r** and **6a^r-b^r**). This observation is in agreement with the MLCT character of the emissive state, as an increase in the negative charge of the sixth ligand results in more repulsion with the dπ orbital, and hence a smaller ΔE between the dπ orbital and the ligand-centered π^* orbital. The change in energy between **5a^r-b^r** and **6a^r-b^r** has a different origin as both groups have the same charge. In the latter case the expected stronger interaction between the Ru-Os ions in the excited state probably results in stabilization of the emissive excited state and hence a lower energy for the photoluminescence.

The only compounds that show no detectable emission at room temperature are the complexes **6a-b** in acetonitrile. As seen in their electronic absorption profiles (Figures 6 and S9), these complexes present a low energy MM`CT state which may be responsible for

the oxidative quenching of the excited state emission. To confirm this hypothesis, the ultrafast dynamics of their transient absorption is being explored in our labs.

Complex Salt	Solvent	L = tpy (a)			L = tpm (b)		
		λ_{em} / nm	$\square_{em}$ x 10^3	τ / ns	λ_{em} /nm	$\square_{em}$ x 10^3	τ / ns
2	ACN	709	0.13	10.4	715	0.23	20.1
5^r	H$_2$O	707	1.42	16.6	720	1.61	15.1
6	ACN	-	<0.01	-	-	<0.01	-
6^r	H$_2$O	725	0.63	9.3	732	0.43	11.8
7^r	ACN	697	0.42	15.6	691	0.61	44.8

Table 6. Emission properties for the complexes reported at 25°C. Monomers **2a** and **2b** from reference 9 are

included for comparison.
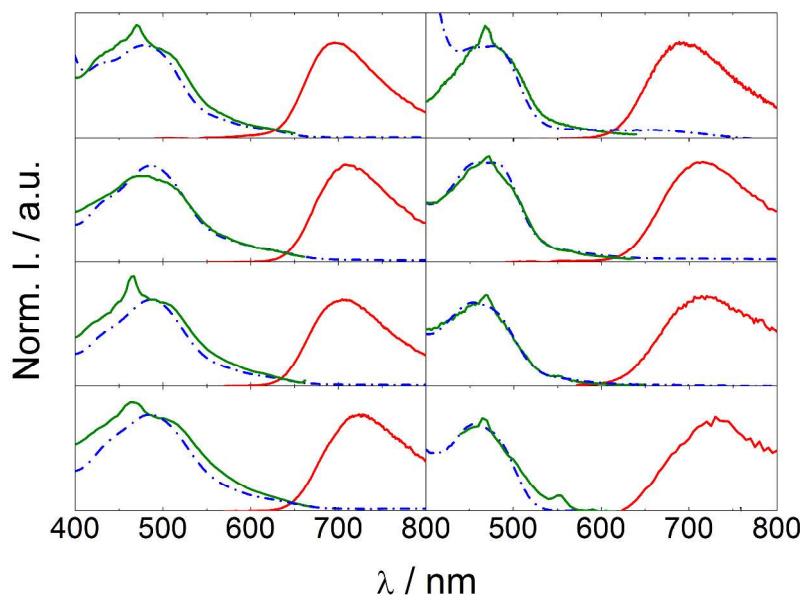
Figure 7. Excitation (green solid line), absorption (blue dashed line) and emission (red solid line) at 25ºC. From top to bottom, left panel: **7a^r** (ACN), **2a** (ACN), **5a^r** (water), **6a^r** (water); right panel: **7b^r** (ACN), **2b** (ACN), **5b^r** (water), **6b^r** (water). Monomers **2a** and **2b** from reference 9 are included for comparison.

The results obtained from photophysical measurements of the bimetallic complexes **5a^r-b^r**, **6a^r-b^r** and **7a^r-b^r** are in line with early reports where multimetal systems containing Ru^{II}(μ-CN)Ru^{II} show no evidence of non radiative deactivation due to the presence of the

additional metallic center,[7,8] but contrast with other reports informing no emission for related systems.[39,45,46]

The origin of the diverse photophysical behavior between closely related cyanide-bridged bimetallic complexes is intriguing. The differences may be traced to the redox potential of the non-emitting metal-center. The lack of emission of the Os(III) containing bimetallic complexes **6a-b** can be easily explained in terms of oxidative quenching, but why two closely related complexes like $[(tpy)(bpy)Ru^{II}(\mu\text{-NC})Ru^{II}(py)_4(CN)]^{2+}$ and $[(tpy)(bpy)Ru(\mu\text{-CN})Ru^{II}(NH_3)_5]^{3+}$ [46] show contrasting photophysical behavior? In these systems, the non-emissive distant Ru(II) could act as an electron donor and reduce the polypyridinic Ru(III) unit present in the MLCT state (reductive quenching). The resulting state has an electron in one polypyridine ligand and a hole in the distant Ru center, hence it creates a remote MLCT state (RMLCT). The energy of this state can be estimated as:

$$E\,(RMLCT) = E(pp/pp^-) - E(RM^{III}/RM^{II})$$

where $E(pp/pp^-)$ is the energy required for the reduction of the polypiridine ligand and $E(RM^{III}/RM^{II})$ is the energy required for the reduction of the distant metal center. The latter values can be replaced by their corresponding redox potentials. This provides only a rough approximation, as the redox potentials are thermodynamic information that also includes solvent effects, but they provide a useful comparison. Hence:

$$E\,(RMLCT) = - [E°\,(pp/pp^-) - E°\,(RM^{III}/RM^{II})]$$

When the energy of the RMLCT lays below the ^{3}MLCT, it can be easily populated leading to deactivation of the otherwise emissive ^{3}MLCT. This is the case for the complexes containing a $Ru^{II}(NH_3)_5$,[39,45,46] which is a good donor, creating a low-energy RMLCT that can act as a quencher state (ESI Figure S11). For the complexes **5a^r-b^r** and **7a^r-b^r**, the non-emissive ruthenium moieties are not so easily oxidized, hence the RMLCT state is

energetically above the ^{3}MLCT and thus it does not become populated. As a result, these complexes show unperturbed emission from the ^{3}MLCT. For the **6a^r-b^r** complexes, we estimate that the RMLCT is close in energy to the ^{3}MLCT, suggesting a partial population transfer to the RMLCT and leading to deactivation of the emissive state. It is interesting to note that the emission quantum yield for the complexes **6a^r-b^r** is smaller than the one observed for the closely related bimetallic complexes **5a^r-b^r**.

Conclusions.

The retention of the photophysical properties observed upon addition of a second metal center indicates an extension of the nuclearity of the complexes without the introduction of competitive non-radiative relaxation pathways. When 1st-row transition metals are used, such as the previously reported Fe and Cr,[9] the presence of low-energy MC (dd) states introduces efficient deexcitation channels. Instead, we show now that by employing 2nd- and 3rd-row transition metals, such as Ru (**5a^r-b^r**, **7a^r-b^r**) and Os (**6a^r-b^r**) we avoid the creation of those deactivation paths. The cyanide and pyridine moieties, classified as high-field ligands in terms of the ligand field theory, may have helped in raising the energy of the MC states. In addition, to prevent deactivation is important to select a metal center that could not open a reductive or oxidative quenching of the ^{3}MLCT.

These findings become critical when the ultimate goal is to prepare polymeric antenna compounds, where there is a requirement of light-absorption followed by transfer of either electronic energy or charge to the reactive center. In those situations, low energy states that may act as energy or charge traps are very undesirable. It is important to note that all the new molecules presented here have exposed cyanide groups, which can be used to further extend their nuclearity. Either additional chromophoric units or actuators can be attached to these complexes, enhancing the absorptivity or introducing a light-dependent function. It is

in this sense that we propose the reported compounds as building blocks for extended polymeric antennae.

Citations

(1)   Hagfeldt, A.; Boschloo, G.; Sun, L.; Kloo, L.; Pettersson, H. *Chem. Rev.* **2010**, *110*, 6595–663.

(2)   Yin, J.-F.; Velayudham, M.; Bhattacharya, D.; Lin, H.-C.; Lu, K.-L. *Coord. Chem. Rev.* **2012**, *256*, 3008–3035.

(3)   Balzani, V.; Credi, A.; Venturi, M. *ChemSusChem* **2008**, *1*, 26–58.

(4)   Alstrum-Acevedo, J. H.; Brennaman, M. K.; Meyer, T. J. *Inorg. Chem.* **2005**, *44*, 6802–27.

(5)   Chakraborty, S.; Wadas, T. J.; Hester, H.; Schmehl, R.; Eisenberg, R. *Inorg. Chem.* **2005**, *44*, 6865–6878.

(6)   Balzani, V.; Sebastiano, B.; Ciamician, C. G.; Bologna, U.; Inorganica, C.; Analitica, C.; Fisica, C.; Messina, U.; Bergamini, G.; Campagna, S.; Puntoriero, F. In *Photochemistry and photophysics of coordination compounds I*; Balzani, V and Campagna, S., Ed.; Springer-Verlag: Berlin, 2007; Vol. 280, pp. 1–36.

(7)   Bignozzi, C. A.; Roffia, S.; Chirboli, C.; Davila, J.; Indelli, M. T.; Scandola, F. *Inorg. Chem.* **1989**, *28*, 4350–4358.

(8)   Scandola, F.; Argazzi, R.; Bignozzi, C. A.; Chiorboli, C.; Indelli, M. T.; Rampi, M. A. *Coord. Chem. Rev.* **1993**, *125*, 283–292.

(9)   Cadranel, A.; Alborés, P.; Yamazaki, S.; Kleiman, V. D.; Baraldo, L. M. *Dalton Trans.* **2012**, *41*, 5343–50.

(10)   Krause, A. *Inorg. Chim. Acta* **1986**, *113*, 161–162.

(11)   Gentil, L. A.; Navaza, A.; Olabe, J. A.; Rigotti, G. E. *Inorg. Chim. Acta* **1991**, *179*, 89–96.

(12)   Alborés, P.; Slep, L. D.; Baraldo, L. M.; Baggio, R.; Garland, M. T.; Rentschler, E. *Inorg. Chem.* **2006**, *45*, 2361–3.

(13)   Coe, B. J.; Meyer, T. J.; White, P. S. *Inorg. Chem.* **1995**, *34*, 3600–3609.

(14)   Llobet, A.; Doppelt, P.; Meyer, T. J. *Inorg. Chem.* **1988**, *27*, 514–520.

(15)   Takeuchi, K. J.; Thompson, M. S.; Pipes, D. W.; Meyer, T. J. *Inorg. Chem.* **1984**, *23*, 1845–1851.

(16)   Armarego, W. L. F.; Perrin, D. D. *Purification of Laboratory Chemicals*; 4th.; Butterworth-Heinemann: Oxford, U.K., 1996.

(17)   Noviandri, I.; Brown, K. N.; Fleming, D. S.; Gulyas, P. T.; Lay, P. A.; Masters, A. F.; Phillips, L. **2006**, 6713–6722.

(18)   Yamamoto, Y.; Tamaki, Y.; Yui, T.; Koike, K.; Ishitani, O. *J. Am. Chem. Soc.* **2010**, *132*, 11743–11752.

(19)   Lebon, E.; Dixon, I. M.; Vendier, L.; Igau, A.; Sutra, P. *Inorg. Chim. Acta* **2007**, *360*, 1235–1239.

(20)   Dixon, I. M.; Lebon, E.; Loustau, G.; Sutra, P.; Vendier, L.; Igau, A.; Juris, A. *Dalton Trans.* **2008**, 5627–35.

(21)   Yang, X.-J.; Drepper, F.; Wu, B.; Sun, W.-H.; Haehnel, W.; Janiak, C. *Dalton Trans.* **2005**, 256–267.

(22)   Nagao, H.; Mizukawa, T.; Tanaka, K. *Inorg. Chem.* **1994**, 3415–3420.

(23)   Adcock, P. A.; Keene, F. R.; Smythe, R. S.; Snow, M. R. *Inorg. Chem.* **1984**, *23*, 2336–2343.

(24)   Rasmussen, S. C.; Ronco, S. E.; Mlsna, D. A.; Billadeau, M. A.; Pennington, W. T.; Kolis, J. W.; Petersen, J. D. *Inorg. Chem.* **1995**, *34*, 821–829.

(25)   Katz, N. E. N.; Romero, I.; Llobet, A.; Parella, T.; Benet-Buchholz, J. *Eur. J. Inorg. Chem.* **2005**, *2005*, 272–277.

(26)   Videla, M.; Jacinto, J. S.; Baggio, R.; Garland, M. T.; Singh, P.; Kaim, W.; Slep, L. D.; Olabe, J. A. *Inorg. Chem.* **2006**, *45*, 8608–8617.

(27) Hartshorn, R. M.; Zibaseresht, R. *Arkivoc* **2006**, *iii*, 104–126.

(28) Coe, B. J.; Meyer, J. T. J.; White, P. S.; Meyer, T. J. *Inorg. Chem.* **1995**, *34*, 593–602.

(29) Pieslinger, G. E.; Alborés, P.; Slep, L. D.; Coe, B. J.; Timpson, C. J.; Baraldo, L. M. *Inorg. Chem.* **2013**, *52*, 2906–17.

(30) Alborés, P.; Slep, L. D.; Weyhermüller, T.; Baraldo, L. M.; Weyhermuller, T. *Inorg. Chem.* **2004**, *43*, 6762–6773.

(31) Rossi, M. B.; Abboud, K. A.; Alborés, P.; Baraldo, L. M. *Eur. J. Inorg. Chem.* **2010**, 5613–5616.

(32) Peters, J. C.; Baraldo, L. M.; Baker, T. A.; Johnson, A. R.; Cummins, C. C. *J. Organomet Chem.* **1999**, *591*, 24–35.

(33) Timpson, C. J.; Bignozzi, C. A.; Sullivan, B. P.; Kober, E. M.; Meyer, T. J. *J. Phys. Chem* **1996**, *100*, 2915–2925.

(34) Rossi, M. B.; Alborés, P.; Baraldo, L. M. *Inorg. Chim. Acta* **2011**, *374*, 334–340.

(35) Macatangay, A. V.; Endicott, J. F. *Inorg. Chem.* **2000**, *39*, 437–46.

(36) Mulliken, R. S. *J. Am. Chem. Soc.* **1952**, *74*, 811–824.

(37) Hush, N. S. *Prog. Inorg. Chem.* **1967**, *8*, 391–444.

(38) Hush, N. S. *Electrochim. Acta* **1968**, *13*, 1005–1023.

(39) Albert, C.; Bignozzi, C. A.; Roffia, S.; Scandola, F. *J. Am. Chem. Soc.* **1985**, *107*, 1644–1651.

(40) Cutin, E. H.; Katz, N. E. *Polyhedron* **1993**, *12*, 955–960.

(41) Siddiqui, S.; Henderson, W. W.; Shepherd, R. E. *Inorg. Chem.* **1987**, *26*, 3101–3107.

(42) Watzky, M. A.; Macatangay, A. V.; VanCamp, R. A.; Mazzetto, S. E.; Song, X. Q.; Endicott, J. F.; Buranda, T. *J. Phys. Chem. A* **1997**, *101*, 8441–8459.

(43) Wong, C.-Y.; Chan, M. C. W.; Zhu, N.; Che, C.-M. *Organometallics* **2004**, *23*, 2263–2272.

(44) Belser, P.; von Zelewsky, A.; Juris, A.; Barigelletti, F.; Balzani, V. *Gazz. Chim. Ital.* **1985**, *115*, 723–729.

(45) Bignozzi, C. A.; Paradisi, C.; Roffia, S.; Scandola, F. *Inorg. Chem.* **1988**, *27*, 408–414.

(46) Ponce, A.; Bachrach, M.; Farmer, P. *Inorg. Chim. Acta* **1996**, *243*, 135–140.